ACS Catalysis

Research Article

pubs.acs.org/acscatalysis

Palladium Nanoparticles Supported in the Nanospaces of Imidazolium-Based Bifunctional PMOs: The Role of Plugs in Selectivity Changeover in Aerobic Oxidation of Alcohols

Babak Karimi,*[,†] Mojtaba Khorasani,[†] Hojatollah Vali,[‡] Carolina Vargas,[§] and Rafael Luque[∥]

[†]Department of Chemistry, Institute for Advanced Studies in Basic Sciences (IASBS), PO Box 45195-1159, Gavazang, Zanjan 45137-6731, Iran

[‡]Department of Anatomy and Cell Biology and Facility for Electron Microscopy Research, McGill University, Montreal, Quebec H3A 2A7, Canada

[§]Departamento de Tecnologia Ambiental (ESCET III), Universidad Rey Juan Carlos, Madrid, Spain

[∥]Universidad de Córdoba, Campus de Rabanales, Edificio Marie Curie (C-3), Ctra Nnal IV-A, Km 396, Córdoba, Spain

Supporting Information

ABSTRACT: Novel heterogeneous catalyst systems comprised of palladium nanoparticles immobilized into the nanospaces of imidazolium-based bifunctional plugged and unplugged periodic mesoporous organosilicas (BFPMO) have been described for the selective aerobic oxidation of alcohols in water. BFPMOs were characterized by N_2 adsorption–desorption analysis, transmission electron microscopy (TEM), powder X-ray diffraction (PXRD), thermal gravimetric analysis (TGA), ^{29}Si and ^{13}C cross-polarization magic angle spinning (CP MAS) NMR spectroscopy, diffuse reflectance infrared Fourier transform spectroscopy (DRIFT), elemental analysis, scanning electron microscopy (SEM), and X-ray photoelectron spectroscopy (XPS). The catalytic activity of all plugged and unplugged catalysts was investigated in the aerobic oxidation of benzylic alcohols by emphasizing the effect of different physiochemical properties as well as the plugs on the reaction selectivity. While unplugged catalysts exhibited much better activity for the selective oxidation of benzyl alcohol to benzaldehyde, the selectivity pattern shifts to the benzoic acid in high yield and selectivity in the presence of plugged catalyst under the exact same reaction conditions. The studies showed for the first time that varying the hydrophobic–hydrophilic balance with concomitant control of plugs in the interior of the mesochannels of the described catalyst enabled tuning of both the catalyst performance and the reaction selectivity, possibly through a cooperative mechanism. A possible model has been proposed to explain this unprecedented observation.

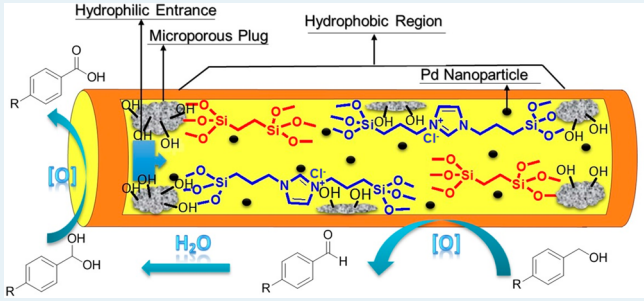

KEYWORDS: *supported palladium, alcohol oxidation, selectivity control, plugged hexagonal templated silica (PHTS), bifunctional periodic mesoporous organosilica (BFPMO), plugged PMO*

INTRODUCTION

Selective oxidation of alcohols into their corresponding carbonyl compounds is a very attractive and challenging transformation from both synthetic and industrial points of view, because the related products are versatile intermediates of valuable compounds, such as pharmaceuticals and agricultural and fine chemicals.[1] In view of stringent environmental issues, green chemistry, and especially atom efficiency, a plethora of research in this area has been recently directed toward the development of new and efficient heterogeneous and recyclable catalysts to accomplish the efficient oxidation of alcohols with molecular oxygen or air as the final oxidant.[2] Along this line, a significant number of metal-catalyzed aerobic oxidation processes based on palladium,[3] platinum,[4] gold,[5] ruthenium,[6] and copper catalysts[7] as well as organocatalysts[8] have achieved promising results. Although the goal of such processes is often to prevent overoxidation in order to stop the reaction at the aldehyde stage, sometimes it is more desirable to produce pure carboxylic acids from alcohols under conditions analogous to those employed for the selective formation of aldehyde. Aldehyde is the first product of this process, whereas carboxylic acids can generally be obtained in two steps in an aqueous medium, via the in situ generation of a *gem*-diol through hydration of aldehyde followed by oxidation into the corresponding carboxylic acid (Scheme 1).[9] Although numerous studies have focused on developing new and eco-friendly catalytic systems on the basis of either transition-metal catalysts or organocatalysts for selective aqueous oxidation of primary

Received: February 4, 2015
Revised: May 22, 2015
Published: May 22, 2015

DOI: 10.1021/acscatal.5b00237
ACS Catal. 2015, 5, 4189–4200

Scheme 1. Possible Pathway for Direct Oxidation of Alcohols to the Related Carboxylic Acids

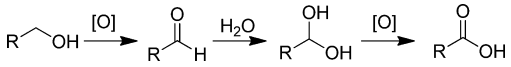

alcohols,[3−8] designing a more sophisticated catalyst system for the selective generation of aldehyde or carboxylic acid remains a challenge. In this context, it was discovered in the aerobic oxidation of primary alcohols catalyzed by Pt/C, that the reaction selectivity could be adjusted to selectively produce aldehydes or carboxylic acids in dioxane or water−dioxane, respectively.[10] However, *the possibility of controlling this reaction to selectively produce aldehyde or carboxylic acid in water under identical reaction conditions has not been explored*. Considering the remarkable difference in lipophilic character of aldehydes and their *gem*-diols, it is conceivable that the reaction selectivity might be controlled to a great extent by adjusting the hydrophobic−hydrophilic balance on the catalyst surface.

The discovery of periodic mesoporous organosilica (PMO) materials has clearly been one of the biggest advances in materials science.[11] These materials are prepared from the hydrolysis and condensation of bridged organosilica precursors $[(R'O)_3Si{-}R{-}Si(OR')_3]$ in the presence of varied surfactant assemblies as the structure directing agent (SDA). In the past decade, hybrid organic−inorganic mesoporous materials including PMOs have been employed in several approaches and strategies in catalysis and catalyst design owing to their well-ordered mesoscopic structure, exceptionally high surface area, high thermal−hydrothermal stability, tunable pore size, and physiochemical properties.[12] Depending on the applications, functionalized silica materials or PMOs with high surface area and available open pore volume are preferred[12] to materials with confined, constricted, and/or sometimes closed pore systems. Nevertheless, functionalized mesoporous materials having constricted channels appeared to be good candidates for specific applications, including selective absorption of organic and important biological compounds, the design of drug delivery systems, and the ability to encapsulate guest molecules with controlled release rates.[13] Van Der Voort et al. reported the first synthesis of periodic mesoporous silica/organosilica with confinement channels: namely, plugged hexagonal templated silica (PHTS) materials.[14] One of the most important features of these materials arose from their nonuniform walls and often constricted pores caused by the microporous silica plugs inside the PHTS channels. The presence and extent of plugs could often be evaluated by N_2 adsorption−desorption analysis.[15] Furthermore, the possibility of plug formation inside the pores of these materials not only provides additional improved stability and an appreciable degree of structure tailorability[16] but also potentially makes the plugged mesoporous materials attractive as encapsulation media for increasing catalytic activity as well as stereoselectivity in some enantioselective reactions through a cooperative confinement mechanism.[17] However, the synthesis of plugged PMOs by employing two bulky groups is quite rare, and to our knowledge the use of plugged PMOs in which the chemical functionality, surface hydrophobic−hydrophilic balance, and plug properties could be tuned for catalytic applications has yet to be explored.

On the basis of our interest in heterogeneous catalysis, we found the selectivity of a number of important chemical transformations could be effectively controlled by adjusting the hydrophobic−hydrophilic balance inside the pores of mesoporous silica materials, where the catalytically active sites are incorporated.[18] We also discovered that monofunctional PMO with bridging imidazolium groups (PMO-IL) can be successfully employed as a powerful functional support for the immobilization and stabilization of metal nanoparticles in various synthetically important transformations.[19] Inspired by the attractive confinement properties around the plugs and within the mesoporous channels, we contemplated whether combining plug technology and built-in bridging functional sites in PMOs might be used to cooperatively control (or adjust) the product selectivity depending on the reaction profile in a certain catalytic transformation.

Although the use of metal nanoparticles and/or metal catalysts, in particular palladium, supported on either functionalized ordered mesoporous materials or PMOs is well-documented in the aerobic oxidation of alcohols,[20] to the best of our knowledge there has not been any study concerning the effect of either surface physiochemical properties or channel plugging of these materials on the selectivity control of this transformation. In this study, we report a novel methodology for the preparation of bifunctional PMOs (BFPMOs) incorporating ionic liquids (ILs) with bridging functional groups (1,4-bis(triethoxysilyl)benzene (BTEB) and 1,4-bis(trimethoxysilyl)ethane (BTME)) featuring highly ordered structures plugging the final materials. In order to prove whether the surface physiochemical properties and plugs could synergistically influence selectivity in the aerobic oxidation of alcohols, we first prepared a set of supported Pd catalysts on the basis of plugged BFPMO-IL, as outlined in Scheme 2. In addition, to discriminate between the fractional influence of the plugs and organic groups (either phenyl or ethyl) on the overall selectivity of the process, two types of supported Pd were prepared: a supported Pd catalyst on a monofunctional PMO-IL comprising only an imidazolium bridge in the PMO framework (Pd@PMO-IL) and a Pd-supported catalyst on an unplugged BFPMO-IL.[21] The catalytic performance of the last two supported Pd catalysts were tested and compared to that of the plugged catalysts in the aerobic oxidation of benzyl alcohol under essentially the same reaction conditions. Preliminary

Scheme 2. Schematic of Plugged (A) and Unplugged (B) Pd Catalysts

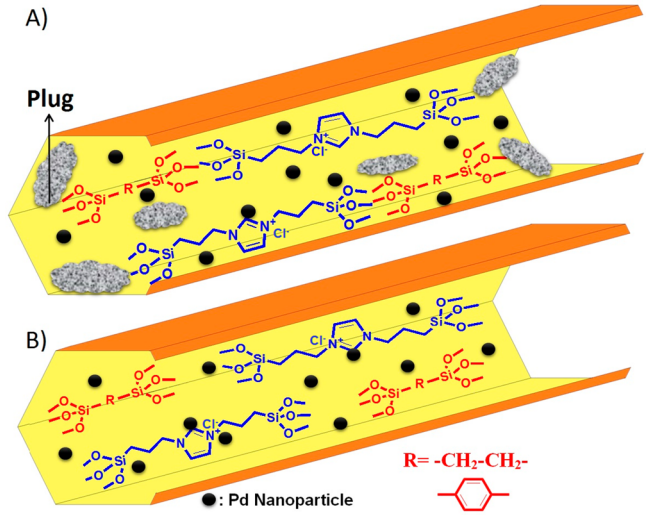

DOI: 10.1021/acscatal.5b00237
ACS Catal. 2015, 5, 4189−4200

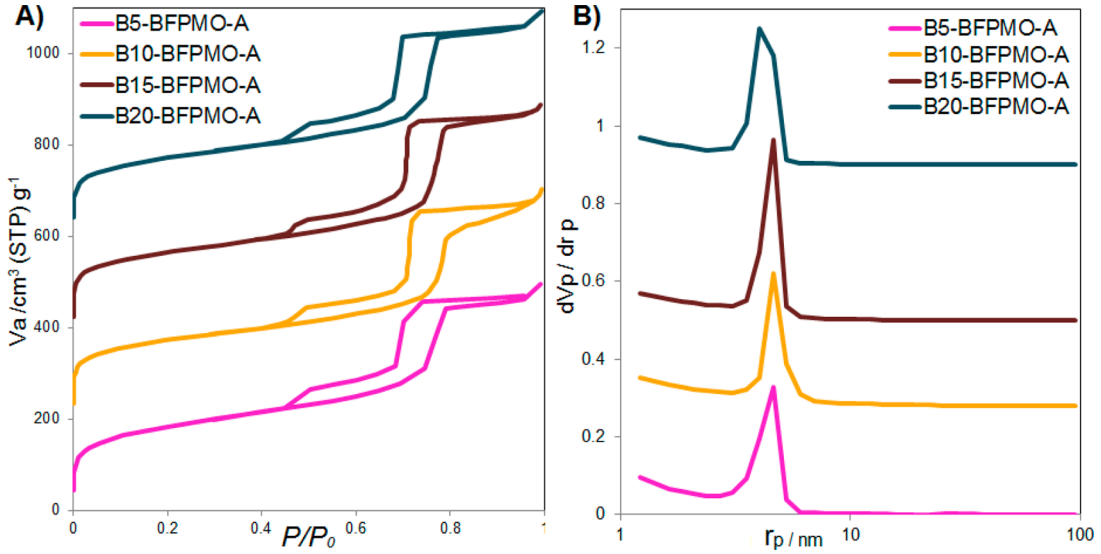

Figure 1. (A) Nitrogen adsorption−desorption isotherms and (B) pore size distributions for B*X*-BFPMO-A (*X* = 5, 10, 15, 20) series. Plots are offset on the vertical axis by 0, 210, 410, and 610 $cm^3\ g^{-1}$ STP and 0, 0.28, 0.5, and 0.9 $cm^3\ g^{-1}\ nm^{-1}$, respectively.

Table 1. Textural Properties of B*X*(5−20)-BFPMO-A and E*X*(5−20)-BFPMO-A Materials Determined from Nitrogen Physisorption and XRD Data[a]

material	organic groups (amt (%))	Si/P123[b]	a_0[c] (nm)	S_{BET}[d] ($m^2\ g^{-1}$)	V_t[e] ($cm^3\ g^{-1}$)	V_{mic}[f] ($cm^3\ g^{-1}$)	D_{BJH}[g] (nm)	w_t[h] (nm)
B5-BFPMO-A	BTEB (5)	80	13.9	611	0.76	0.07	9.2	4.7
B10-BFPMO-A	BTEB (10)	83	13.0	518	0.73	0.09	9.2	3.8
B15-BFPMO-A	BTEB (15)	87	13.1	529	0.73	0.08	9.2	3.9
B20-BFPMO-A	BTEB (20)	90	13.1	569	0.73	0.11	8.1	5.0
E5-BFPMO-A	BTME (5)	80	13.8	604	1.20	0.06	10.6	3.2
E10-BFPMO-A	BTME (10)	83	13.7	530	0.94	0.07	10.6	3.1
E15-BFPMO-A	BTME (15)	87	13.3	539	0.87	0.07	9.2	4.1
E20-BFPMO-A	BTME (20)	90	13.7	569	0.91	0.08	9.2	4.5

[a]All materials contained 10% IL precursors and were also synthesized according to method A, as described in the Supporting Information. [b]Total amount of Si in TMOS, BTEB (or BTME), and IL precursors in mmol. [c]a_0 = unit cell derived from d_{100} values using $a_0 = 2d_{100}/\sqrt{3}$. [d]S_{BET} = specific surface area was determined from the linear part of the BET plot ($P/P_0 \approx 0.05-0.15$). [e]V_t = total pore volume on the basis of N_2 adsorbed at $P/P_0 \approx 0.995$. [f]V_{mic} = micropore volume calculated by the t-plot method. [g]D_{BJH} = pore size distribution calculated from the adsorption branch using BJH methods (may underestimate values of mesopores). [h]w_t = pore wall thickness calculated using $w_t = a_0 - D_{BJH}$ (may underestimate values of pore wall thickness).

investigations showed both the hydrophobic−hydrophilic balance and plug formation inside the pores of these plugged catalysts have a remarkable effect on the efficiency as well as the selectivity of the title reaction under the described reaction conditions.

RESULTS AND DISCUSSION

Four phenyl-BFPMOs (denoted as B*X*--BFPMO-A, where B, X, and A indicate phenyl, phenyl content, and method A, respectively) were first synthesized with organic contents ranging from 5 to 20% BTEB and 10% 1,3-bis(3-trimethoxysilylpropyl)imidazolium chloride (BTMSPCl) precursors:[22] i.e., all silica precursors such as the bridged ionic liquid (BTEB) and tetramethoxyorthosilicate (TMOS) were simultaneously added into the solution.[21] N_2 adsorption−desorption isotherms and BJH (Barrett−Joyner−Halenda) pore size distributions for all BFPMOs are summarized in Figure 1. Nitrogen adsorption isotherms for all synthesized materials exhibited a type IV isotherm with a sharp capillary condensation step at relative pressure (P/P_0) of 0.6−0.7, which confirmed the uniformity of cylindrical mesoporous channels in the materials (Figure 1A). Interestingly, N_2 desorption isotherms showed two steps similar to those reported for PHTS materials (sub step at $P/P_0 \approx 0.45$). Such adsorption−desorption isotherms are very similar to those of materials having both open and plugged cylindrical mesopores. Open pores are gradually desorbed at reduced relative pressures, but blocked pores will remain filled until the vapor pressure is lowered to $P/P_0 \approx 0.45$ (lower limit for hysteresis P/P_0), at which point condensed N_2 eventually desorbs. While the first segment of the N_2 desorption branch provides information on open pores, the last segment can used to evaluate the pore size distribution in confined and plugged sections.[23] The results are in good agreement with those in the published literature.[14,15] Calculations from the adsorption branch using the BJH method (Figure 1B) show that plugged B-BFPMOs have a very narrow pore size distribution, with a small fraction of pore constriction. Increasing the Si/P123 molar ratio leads to a decrease in both pore size distribution and pore volume (from 9.2 to 8.0 nm and from 0.85 to 0.73 $cm^3\ g^{-1}$, respectively). The micropore volume systematically increased from 0.07 to 0.11 $cm^3\ g^{-1}$ by the very gradual growth of microplugs in the B-BFPMO pores, remarkably similar to that reported for PHTS.[14,15] Other textural properties determined by N_2 physisorption and X-ray

DOI: 10.1021/acscatal.5b00237
ACS Catal. 2015, 5, 4189−4200

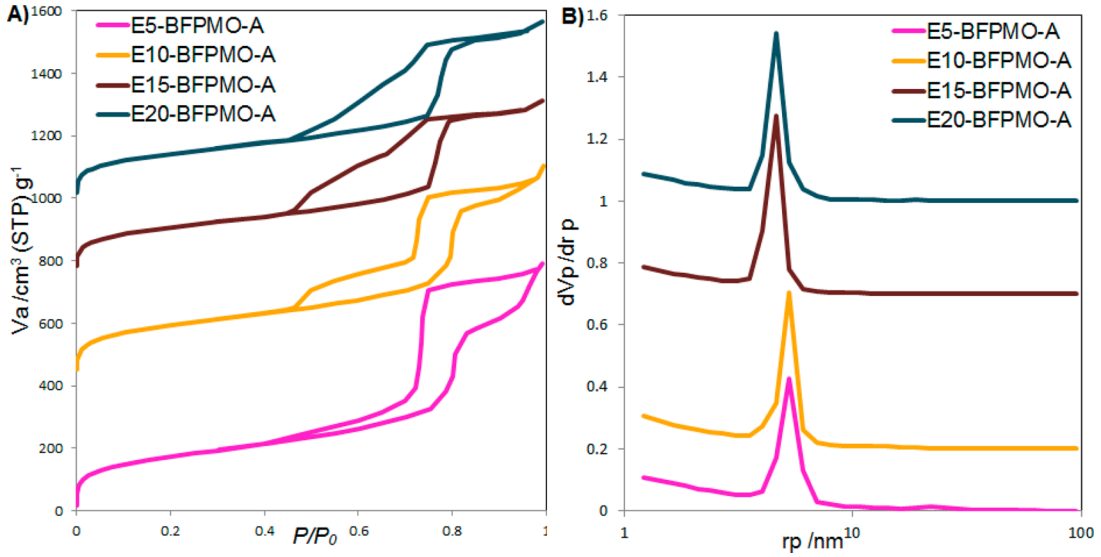

Figure 2. (A) Nitrogen adsorption−desorption isotherms and (B) pore size distributions for E*X*-BFPMO-A (*X* = 5, 10, 15, 20) series. Plots are offset on the vertical axis by 0, 420, 750, and 975 $cm^3\ g^{-1}$ STP and 0, 0.2, 0.7, and 1.0 $cm^3\ g^{-1}\ nm^{-1}$, respectively.

diffraction (XRD) data, including BET area (S_{BET}), unit cell (a_0), and pore wall thickness (w_t) for all B*X*-BFPMO-A samples are summarized in Table 1. Estimated BET area and wall thickness values vary from 518 to 569 $m^2\ g^{-1}$ and from 3.8 to 5.5 nm, respectively. Overall, the textural properties and shapes of the resulting isotherms suggested that the natures of plugging are likely very similar for all synthesized B-BFPMOs (Figure 1A).

In the next stage, four ethane-containing BFPMO-As were also synthesized with various organic contents ranging from 5 to 20% (denoted as E*X*(5−20)-BFPMO-A). N_2 adsorption−desorption isotherms and pore size distributions for these materials have also been determined and are summarized in Figure 2. A remarkable increase in plugging was observed in these materials with increasing ethane contents. Plugging was strongly enhanced by increasing the Si/P123 molar ratio in E-BFPMO, as suggested by the broad hysteresis loop with a moderately delayed capillary evaporation step, which may be attributed to microplugs with distributed particle size. These observations are consistent with other reports on the synthesis of PHTS materials prepared by increasing Si/P123 molar ratios.[14−16] However, the reason for the different behaviors of BTME and BTEB in creating plugs is not clear for us at this stage and we are currently working to find a logical explanation. All E-BFPMOs exhibited very narrow pore size distributions and highly ordered mesostructures regardless of the observed plugging and the presence of a significant proportion of confined pores at high Si/P123 molar ratios (Figure 2B). Related textural properties for all E-BFPMO materials are summarized in Table 1. Predictably, pore size distribution, specific surface area, and pore volume for these materials decreased from 10.6 to 9.2 nm, from 604−539 $m^2\ g^{-1}$ and from 1.2 to 0.87 $cm^3\ g^{-1}$ with an increase in ethane content, respectively. Microporosity and wall thickness were found to systematically increase from 0.06 to 0.08 $cm^3\ g^{-1}$ and from 3.1 to 4.5 nm, respectively, which are in good agreement with those in the published literature for PHTS materials. These findings may be attributed to the presence of microplug encapsulation or nonuniformity in the walls at increasing Si/P123 molar ratios.

It should be noted that we have conducted the synthesis of all materials under strongly acidic conditions (pH <0.1) in order to ensure that silica precursors are immediately converted to their corresponding hydrolyzed species as soon as their methanolic mixtures (solutions) were added into the initial HCl/Pluronic solution. Methanol was highly beneficial for adjusting the rate (slowing down) of co-condensation of the precursors.[14c,d] It also suppressed excessive nontemplated polymerization in highly acidic solutions, ensuring the formation of a well-ordered structure and homogeneous distribution of all precursors inside the PMO framework.

Transmission electron microscopy (TEM) images of B- and E-BFPMO-A materials are shown in Figures 3 and 4,

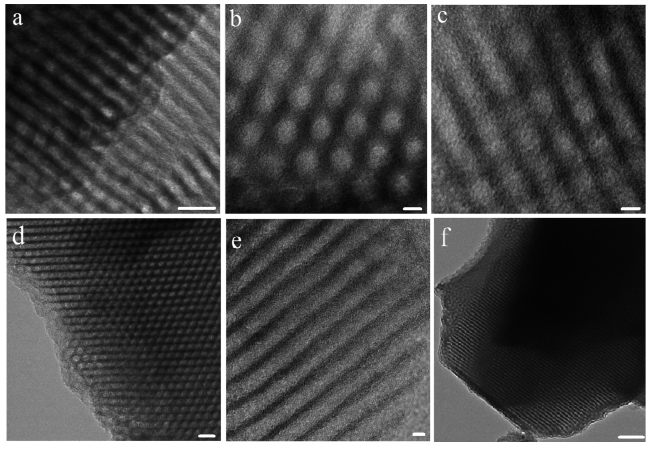

Figure 3. TEM images of (a) B5-BFPMO-A (scale bar 5 nm), (b, c) B10-BFPMO-A (scale bar 5 nm), (d, e) B15-BFPMO-A (scale bars 20 and 5 nm, respectively), and (f) B20-BFPMO-A (scale bar 100 nm).

respectively. The materials exhibited a highly ordered structure with well-defined cylindrical, 2D-hexagonal pores, in good agreement with results obtained by N_2 physisorption analysis. Ordered nanostructures preserved the long-range ordering even at large loadings of functional groups (up to 30%, B20-BFPMO-A, Figure 3f) or E20-BFPMO-A (Figure 4d). Energy dispersive X-ray spectroscopy (EDS) of the solvent extracted B-

DOI: 10.1021/acscatal.5b00237
ACS Catal. 2015, 5, 4189−4200

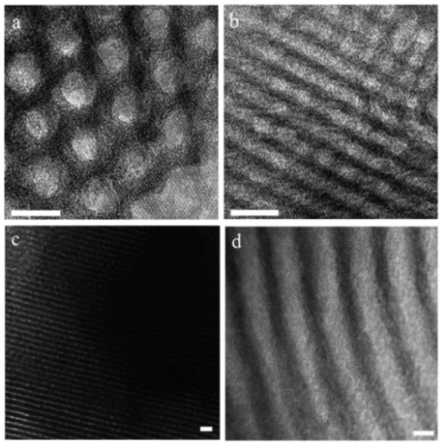

Figure 4. TEM images of (a) E5-BFPMO-A (scale bar 10 nm), (b) E10-BFPMO-A (scale bar 10 nm), (c) E15-BFPMO-A (scale bar 25 nm), and (d) B20-BFPMO-A (scale bar 5 nm).

or E-BFPMO-A materials did not show traces of KCl residue (Figures S3−S10 in the Supporting Information), suggesting that KCl (used in the synthesis) did not contribute as a plugging agent.[17a]

Powder X-ray diffraction (PXRD) analysis was also carried out on both phenyl- and ethyl-containing BFPMO-A (Figures S11 and S12 in the Supporting Information). Interestingly, the XRD patterns of all samples exhibited three peaks with a d value ratio of $1:(1/\sqrt{3}):(1/2)$ that can be indexed as d_{100}, d_{110}, and d_{200} reflections of the highly ordered 2D hexagonal symmetry ($P6mm$), respectively.[24] These findings are in good agreement with the N_2 adsorption−desorption data and TEM images. Moreover, no KCl peaks were observed in the diffractogram over the range 20−70° 2θ (Figure S13 in the Supporting Information), which clearly indicated successful removal during P123 extraction with acidic ethanol.[17a]

The integrity of the organic functional groups in the framework of the materials was studied by ^{13}C cross-polarization magic angle spinning (CP-MAS) NMR spectroscopy. Figure S14 in the Supporting Information shows the solid-phase NMR spectrum of E15-BFPMO-A. Examination of this spectrum clearly leads to the conclusion that both ethyl and propyl imidazolium fragments remained intact during the preparation and template removal stages. Notably, all six peaks that one might expect for E15-BFPMO-A are observed. The ^{13}C CP-MAS NMR spectrum for E15-BFPMO-A shows a resonance peak at 4.8 ppm, which is attributed to the methylene carbons in the ethane bridge (Figure S14B). The peaks at 9.4, 24.2, and 52.4 ppm are attributed to C3, C2, and C1 in the propyl groups bridged to the imidazolium ring and Si atoms in the E15-BFMPO-A framework.[22,25] The signals at 123.4 and 135.9 ppm arise from carbons in CHCH and NHCN of the imidazolium ring, respectively. Moreover, no additional carbon peaks were detected in ^{13}C CP-MAS NMR of E15-BFPMO-A. This suggests that all of the Si−C bonds were retained during the synthesis and surfactant extraction stages. However, the presence of two weak peaks at ∼70 and ∼73 ppm in the ^{13}C CP-MAS NMR spectra of our E10-BFPMO-A sample are attributed to carbons of the surfactant residue (marked by asterisks in Figure S14A), which likely remained in the samples during the surfactant extraction by ethanol.[26] The peak at 4.8 ppm tends to be enhanced by increasing the content of BTME with respect to that of BTMSPCl in the bifunctionalized samples E10-BFPMO-A, E15-BFPMO-A, and E20-BFPMO-A. Figure S14D shows a typical ^{13}C CP-MAS NMR spectrum of the bifunctionalized sample B20-BFPMO-B. A sharp peak at 133.7 ppm with side bands of phenyl carbons overlaps with the resonance from carbons in the NCHN of the imidazolium moiety. The spectrum also exhibits four resonances at 123.1, 52.5, 24.0, and 9.6 ppm that are characteristic of CHCH in imidazolium rings and C1, C2, and C3 carbons of the propyl bridges. The weak peak at ∼75 ppm is likely due to the carbons of the Pluronic P123 residue.[26] However, this spectrum also suggests that organic precursors such as BTEB and BTMSPCl have been embedded in the BFPMO framework.

^{29}Si NMR CP-MAS NMR spectroscopy experiments were carried out to evaluate the incorporation of organic groups, i.e. imidazolium, phenyl, and ethyl groups, inside the pore walls of the BFPMO-As (Figures S15 and S16 in the Supporting Information). ^{29}Si NMR spectra of all phenyl-PMO-A materials displayed three distinctive peaks at δ −59.5, −68, and −78 ppm, which are attributed to Si species covalently bonded to carbon atoms T^1 (C-**Si**-(OSi)$(OH)_2$), T^2 (C-**Si**-$(OSi)_2(OH)$), and T^3 (C-**Si**-$(OSi)_3$), respectively.[27] E-BFPMO-A spectra jointly display two signals at −58 and −65 ppm that correspond to Si atoms covalently bonded to carbon atoms T^2 (C-$SiO_2(OH)$) and T^3 (C-SiO_3), respectively.[27] The absence of a T^1 signal in E-BFPMO confirmed that the degree of network condensation for these materials is larger in comparison to that of B*X*-BFPMO materials. Furthermore, ^{29}Si NMR spectra for all BFPMOs show three peaks at δ −91, −100, and −109 ppm, related to Q^2[**Si**-$(OSi)_2(OH)_2$], Q^3[**Si**-$(OSi)_3(OH)$], and Q^4[**Si**-$(OSi)_4$] silica network species, respectively.[28] The degree of framework condensation was found to be high ,as evidenced by the higher percentage of fully cross-linked T^3 and Q^4 silicon sites. Comparison of the solid-state ^{29}Si NMR spectra (Figures S15 and S16 and Table S1 in the Supporting Information) shows that, with increasing content of BTEB or BTME in the initial gel, the intensity of T^n bands with respect to Q^n bands gradually increased, which illustrates successful condensation and incorporation of IL moieties into the mesoporous walls.

The presence of organic groups in the materials was also confirmed by diffuse reflectance infrared Fourier transform spectroscopy (DRIFT) measurements (Figures S17−S19 in the Supporting Information). All phenyl- or ethyl-BFPMO-As exhibited similar patterns, with differences only in peak intensity. Sharp and wide peaks appeared at ca. 925 and 1096 cm^{-1}, corresponding to asymmetric and symmetric stretching vibrations of Si−O−Si bonds.[29] The peak at 3125 cm^{-1} may be assigned to the asymmetric stretching vibration of C−H in the phenyl ring and/or imidazole groups.[30] Ethyl and propyl functional groups in BFPMO-A contribute with several peaks in the 2930−3059 cm^{-1} range (aliphatic C−H stretching).[29] Moreover, the presence of the imidazolium functionality can be generally confirmed by peaks at 1620 cm^{-1} that are assigned to the stretching vibrations of C═N bonds.[30] Additionally, the bands at 1560 cm^{-1} which correspond to the stretching vibrations of C═C bonds confirmed the presence of phenyl groups in the materials.[30] Peaks at 700−750 and 3300 cm^{-1} can be ascribed to bending vibrations of Si−C bonds and stretching vibrations of O−H in surface silanol groups,[30,31] respectively, which in addition to the aforementioned peaks confirmed the stability of PMO precursors during the sol−gel process, aging, and surfactant extraction stages.

DOI: 10.1021/acscatal.5b00237
ACS Catal. 2015, 5, 4189−4200

Table 2. Chemical and Physical Properties of Catalysts Used in Screening Studies[a]

entry	cat. name	FG (amt (%))[b]	S_{BET}[c] ($m^2\ g^{-1}$)	V_t[d] ($cm^3\ g^{-1}$)	D_{BJH}[e] (nm)	Pd[f] (mmol g^{-1})
1	Pd@U-B20[g]	B (20)	400	0.5	10.6	0.085
2	Pd@U-E10[h]	E (10)	371	0.82	10.6	0.096
3	Pd@U-E15	E (15)	395	0.83	10.6	0.086
4	Pd@P-E10[i]	E (10)	450	0.88	10.6	0.080
5	Pd@P-E15	E (15)	378	0.67	9.2	0.084
6	Pd@P-E20	E (20)	452	0.78	9.2	0.085

[a]All materials contained 10% bridged IL and were synthesized according to either method A (plugged) or B (unplugged), as described in the Supporting Information. [b]Bridge functional group. [c]S_{BET} = specific surface area determined from the linear part of the BET plot ($P/P_0 \approx 0.05-0.15$). [d]V_t = total pore volume based on the N_2 adsorbed at $P/P_0 \approx 0.995$. [e]D_{BJH} = pore size distribution calculated from the adsorption branch using BJH methods. [f]Loading of Pd in the either plugged or unplugged catalyst as determined by ICP-AES of acid-washed sample. [g]U = unplugged catalyst and B = phenyl functional group. [h]E = ethyl functional group. [i]P = plugged catalyst.

The thermal stability of BFPMO-A was evaluated by thermal gravimetric analysis (TGA). TG patterns of synthesized materials were recorded in the range of 25−800 °C (Figures S20−S27 in the Supporting Information). The first weight loss (ca. 5−8%, below 100 °C) can be correlated to physisorbed water and alcohol desorption occluded in the pores or on the surface of the materials. Phenyl-containing materials have been proved to be slightly more stable in comparison to their ethyl-containing counterparts owing to the insignificant weight loss between 100 and 300 °C.[32] In any case, all BFPMO-As exhibited high thermal stability, with total measured weight loss of organic functional groups totally removed at temperatures >400 °C as measured by TGA, which is in close agreement with theoretical organic loadings and elemental analysis data (Table S2 in the Supporting Information). These data clearly revealed that all of the bridged precursors were preserved after the sol−gel process and even after extraction of SDA under acidic ethanol conditions. These findings were also in good agreement with results from ^{29}Si CP-MAS NMR (Figures S15 and 16 in the Supporting Information).

Elemental analysis (CHN) was carried out to evaluate the integrity of the organic bridging functional groups inside the framework of our materials. As can be seen in Table S2 in the Supporting Information, the weight percentage of carbon increase in accord with the nitrogen percentages decreased with an increase in either the BTME or BTEB content in the E*X*(5−20)-BFPMO-A and B*X*-(5−20)-BFPMO-A series, respectively, which again confirms the incorporation of all bridging groups into the framework of the materials.

Finally, a set of supported Pd catalysts based on our plugged BFPMO-IL were successfully prepared by replacing the chloride ions in the parent BFPMO with $PdCl_4^{2-}$ using a modified ion exchange technique (Scheme 2).[33] In addition, to discriminate between the fractional influence of the plugs and organic groups (either phenyl or ethyl) on the overall selectivity of the aerobic oxidation of alcohols (vide infra), a set of Pd-supported catalysts based on unplugged BFPMO-IL (Pd@U-B20, Pd@U-E10, and Pd@U-E15) with very close metal loadings were also prepared by adjustment of the synthesis conditions (stepwise addition of silica precursors).[21] Using inductively coupled plasma-atomic emission spectroscopy (ICP-AES) of acid-washed samples, the amount of Pd in either synthesized plugged or unplugged catalysts was determined to be in the range 0.08−0.096 mmol g^{-1} (Table 2).

The catalytic activity of all catalysts (0.5 mol %) was first examined in the aerobic oxidation of benzyl alcohol by using water as a green solvent at 90 °C. In our earlier study, we showed that Pd nanoparticles supported on monofunctional PMO-IL (Pd@PMO-IL) was an effective catalyst for the selective oxidation of alcohols to the corresponding carbonyl compound with trifluorotoluene (TFT) as the solvent.[34] However, this catalyst exhibited ineffective catalytic activity in an aqueous medium (Table 3, entries 1 and 2). Therefore, the

Table 3. Aerobic Oxidation of Benzylic Alcohols Catalyzed by Unplugged Pd@BFPMO[a]

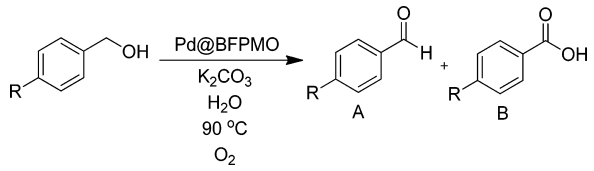

entry	R	cat.	T (h)	conversion (%)	amt (%)[b] A	amt (%)[b] B
1[c]	H	Pd@PMO-IL	24			
2[d]	H	Pd@PMO-IL	24	14	14	
3	H	Pd@U-B20	15	43	43	
4	H	Pd@U-E10	15	44	44	
5	H	Pd@U-E15	15	90	90	
6	CH_3	Pd@U-E15	15	95	95	
7	OCH_3	Pd@U-E15	15	>99	>99	
8	Cl	Pd@U-E15	15	79	74	<5
9[e]	H	Na_2PdCl_4	24			

[a]Reaction conditions: 0.5 mmol of alcohol, 1.5 mmol of K_2CO_3, 1 atm of O_2, 0.5 mol % of catalyst, and 1.5 mL of H_2O at 90 °C. [b]GC yield using internal standard method. [c]Pd catalyst based on monofunctional PMO-IL at 80 °C.[36] [d]At 90 °C.[36] [e]0.5 mol % of Na_2PdCl_4 was used.

unplugged catalyst Pd@U-B20, which contained up to 20% phenyl groups, was evaluated under the same reaction conditions. This reaction produced 43% benzaldehyde after 20 h (Table 3, entry 3). These results suggest that the presence of the phenyl groups inside the nanospaces of the unplugged BFPMO framework plays a decisive role in improving catalytic activity, likely by enhancing the surface hydrophobicity, which in turn favors faster diffusion of benzyl alcohol into the mesoporous channels where the Pd species are located. To obtain further insight into this issue, we investigated whether the use of BFPMOd having appropriate concentrationd of ethyl functional groups would result in a similar catalyst improvement. Although the aerobic oxidation of benzyl alcohol in the presence of Pd@U-E10 (0.5 mol %) comprised of 10% imidazolium and 10% ethyl functional groups inside the framework (E10-BFPMO-A) produced 44% benzaldehyde yield within 15 h at 90 °C (Table 3, entry 4), the same

DOI: 10.1021/acscatal.5b00237
ACS Catal. 2015, 5, 4189−4200

reaction using Pd@U-E15 (0.5 mol % as well) with 10% and 15% imidazolium and ethyl functionalities, respectively, furnished 90% benzaldehyde yield and an excellent selectivity of >99% (Table 3, entry 5). Considering the hydrophobic nature of PMOs through the sequence ethylene > phenylene > methylene > silica,[35] the outstanding catalytic performance of Pd@U-E15 might be due to the hydrophobic−hydrophilic balance arising from the ethyl units inside the mesochannels of the unplugged BFPMO-IL support. This in turn favors easier diffusion of the starting alcohol into the nanospace of the catalyst, thereby enhancing the catalytic activity Pd@U-E15 under the described aqueous reaction conditions. Encouraged by these promising results, we then directed our attention toward the oxidation of some substituted benzylic alcohols in water. *p*-Methoxybenzyl and *p*-methylbenzyl alcohols were oxidized to the corresponding aldehydes in excellent yields and selectivities without any overoxidation to the carboxylic acids (Table 3, entries 6 and 7). Moreover, *p*-chlorobenzyl alcohol was also oxidized to the related aldehyde with good yield and high selectivity (Table 3, entry 8). In particular, unsupported catalyst (Na_2PdCl_4) with the same catalytic loading displayed no activity under identical reaction conditions (Table 3, entry 9). These data imply that the presence of hydrophobic groups (ethyl moiety) and the active catalyst in its immobilized form is indispensable to attaining high activity in water by employing the present catalyst system.

What is appealing in these investigations is that, despite the use of water as the reaction solvent, the amount of the byproduct benzoic acid remained below 5% even after prolonged reaction times at 90 °C and under a pure O_2 atmosphere in the presence of unplugged Pd@U-E15 (Table 3, entry 8). Therefore, we next investigated whether the confinement effect caused by the plugged mesopores as well as the physiochemical properties in the proximity of the plugs could also synergistically contribute to the selectivity of aerobic oxidation of alcohols under the present reaction conditions.

Three supported Pd catalysts with approximately the same Pd loadings were prepared via simple impregnation of plugged E20-BFPMO-A, E15-BFPMO-A, and E10-BFPMO-A with an aqueous solution of Na_2PdCl_4 to produce the corresponding plugged catalysts Pd@P-E20, Pd@P-E15, and Pd@P-E10 (Table 2), respectively, in a way similar to that previously described for the preparation of unplugged catalysts (Scheme 2). It is worth noting that the extent of the plugging in these catalysts was estimated to be in the order Pd@P-E20 ≈ Pd@P-E15 > Pd@P-E10, as evidenced by N_2 sorption analysis. In addition, no apparent loss of N_2 adsorption−desorption isotherms was found upon Pd incorporation within the indicated range of Pd content in the materials, suggesting the mesoporous structure and degree of plugging of the materials was mainly preserved under the described doping conditions (Figures S32−S42 in the Supporting Information). The choice of pristine plugged bifunctional PMOs was motivated by the initial promising results obtained with the supported Pd catalyst on the ethyl functionalized BFPMO-IL (catalyst Pd@U-E15) in the aerobic oxidation of alcohols (Table 3). Therefore, in order to understand how plugs may impact the selectivity of the process, plugged ethyl-bridged BFPMO-IL was employed as the support for the remainder of the study.

After initial characterization of the plugged catalysts Pd@P-E10, Pd@P-E15, and Pd@P-E20 (Figures S32−S42 in the Supporting Information), their catalytic performance (0.5 mol % of Pd) was tested and compared in the aerobic oxidation of benzyl alcohols under essentially the same optimized reaction conditions presented in Table 3 for the unplugged catalysts Pd@U-B20, Pd@U-E10, and Pd@U-E15. Unless otherwise noted, to compare the performance (both selectivity and reactivity) of all catalysts, the reaction time was fixed at 15 h. Interestingly, while the oxidation of benzyl alcohol in the presence of Pd@P-E10 (0.5 mol %) having 10% ethyl bridges afforded 76% conversion, the yield of benzaldehyde dropped to 30% with concomitant formation of benzoic acid at a 46% yield (Table 4, entry 1). Catalyst Pd@P-E15 with a slightly higher

Table 4. Aerobic Oxidation of Benzylic Alcohols Catalyzed by Plugged Pd@BFPMO[a]

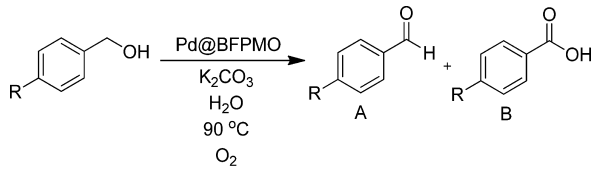

entry	R	cat.	T (h)	conversion (%)	amt (%)[b] A	amt (%)[b] B
1	H	Pd@P-E10	15	76	30	46
2	H	Pd@P-E15	15	95	2	93
3	CH_3	Pd@P-E15	24	>99	25	75
4	OCH_3	Pd@P-E15	24	>99	40	60
5	Cl	Pd@P-E15	20	>99	14	86
6	H	Pd@P-E20	15	>99	21	78
7	CH_3	Pd@P-E20	24	88	35	53
8	OCH_3	Pd@P-E20	24	85	35	50
9	Cl	Pd@P-E20	24	74	5	69

[a]Reaction condition: 0.5 mmol of alcohol,1.5 mmol of K_2CO_3, 1 atm of O_2, 0.5 mol % of catalyst, and 1.5 mL of H_2O at 90 °C. [b]GC yield using the internal standard method of calibration.

ethyl content (15%) in the mesoporous network exhibited improved activity, leading to a 95% benzyl alcohol conversion (Table 4, entry 2). There was, however, a noticeable change in product selectivity in comparison to that of the unplugged catalyst Pd@U-E15 (Table 3, entry 5) having almost the same ethyl loading under essentially identical reaction conditions. Hence, we suspected here that the key factor explaining the remarkable selectivity difference between Pd@U-E15 and Pd@P-E15 might be ascribed to the presence of plugs inside the mesochannels of Pd@P-E15. This surprising difference in behavior between two catalyst systems encouraged us to further investigate the possible synergistic role of plugs and organic (ethyl) bridges in our system. This was further stimulated by the fact that effective methods for the direct oxidation of benzylic alcohols into their benzoic acids in the presence of Pd catalysts are extremely rare,[36] since it has been well-postulated that even a low concentration of benzyl alcohol can effectively inhibit the overoxidation of benzaldehyde into benzoic acid.[37] Therefore, our next step was to determine whether the observed product selectivity could be produced by applying plugged catalyst Pd@P-E15 under the same reaction conditions for the oxidation of a range of benzylic alcohols similar to that demonstrate in Table 3 (Table 4, entries 3−5). It was found that the enhanced benzoic acid formation could also be achieved in water suggesting the presence of plugs in catalyst Pd@P-E15 might indeed have some marked impact on the reaction selectivity (Table 4, entries 3−5). To collect more

DOI: 10.1021/acscatal.5b00237
ACS Catal. 2015, 5, 4189−4200

information on the synergistic role of plugs and ethyl bridge in our system, the oxidation of the same range of alcohols was carried out using catalyst Pd@P-E20 having 20% ethyl moiety in the mesoporous network (~5% higher ethyl concentration than of Pd@P-E15) under the same reaction conditions (Table 4, entries 6–9).

By increasing the ethyl bridge content in the material, a meaningful improvement in the overall consumption of starting alcohols (up to >99% conversion) was observed. This is due to the gradual increase in alcohol diffusion into the system pore space that likely arises from a favorable interaction of the hydrophobic corona of alcohol molecules with the hydrophobic mesopores of the catalyst. Although consideration of this interaction helps to explain the relationship between the degree of hydrophobicity of the mesochannels in our catalysts based on the ethyl bridge-plugged BFPMO-ILs and their catalytic performance (i.e benzyl alcohol conversion) in water, it does not explain the increased selectivity to benzoic acid derivatives when the ethyl content was increased from 10 to 15% and the noticeable drop when the content was increased to 20%. By comparing the data in Table 3 and 4 of the oxidation of primary benzylic alcohols using unplugged (Pd@U-E15) and plugged catalysts (Pd@P-E15), respectively, we speculated that while an appropriate concentration of ethyl bridge in our system was indispensable to ensuring acceptable conversion, the presence of plugs resulted in a dramatic shift in reaction selectivity to the benefit of benzoic acid generation. There was the critical consideration of how the plug characteristics and the physicochemical nature of the nanospaces in the mesoporous solid Pd@P-E15 as well as the reaction profile could be rationalized. It is well-known that, in the preparation of plugged SBA-15, plugs can form at high TEOS (tetraethoxyorthosilicate)/template ratios,[14] as was the case in the synthesis of our materials. This would suggest that the plugs in our materials mainly consisted of amorphous silica nanocapsules likely originating from the hydrolysis and condensation of TEOS. Hence, it is reasonable to assume that the silica nanocapsules have a high surface concentration of silanol groups which provide markedly *hydrophilic nanoregions* inside the hydrophobic mesochannels of the BFPMO-IL (Scheme 3). In considering the reaction profile of alcohol oxidation (Scheme 3), we hypothesized that a hydrophilic *nanoregion* can strongly interact with hydrated aldehyde (*gem*-diol), presumably through hydrogen-bond interactions. As a consequence, it appears that the presence of plugs in the interior of the nanospaces of catalyst Pd@P-E15 would enable a longer retention of hydrated aldehyde inside the system pore space in close proximity to the available Pd active site, which thus overoxidized to produce the corresponding acid. This model may also explain the consistent decrease in selectivity of benzoic acid formation when the more hydrophobic Pd@P-E20 (with 20% ethyl bridge) is used rather than the catalyst Pd@U-E15. At an ethyl bridge content >15% (i.e. ~20%), the hydrophobic nature of the catalyst becomes dominant, rendering the mesoporous environment less favorable to interact with the hydrated aldehydes and prohibiting to some extent penetration of the hydrated aldehyde into the pore system. This would certainly decrease the concentration of hydrated aldehyde in the proximity of active sites, thereby limiting the formation of acidic products and leading to a drop in the reaction selectivity toward the formation of carboxylic acid. On the basis of this model, the excellent selectivity toward aldehyde formation in the case of unplugged catalyst Pd@U-E15 might be attributed to the pronounced hydrophobic character of the open pore system in Pd@U-E15, which makes diffusion of hydrated aldehyde from the aqueous phase into the mesopores more difficult, thus lowering its overoxidation to the corresponding carboxylic acids. The role of the physiochemical and structural characteristics of the described material in reaction selectivity was further confirmed by the lack of detectable oxidation products in the control experiments in the absence of either plugged or unplugged BFPMO-IL (Table 3, entry 9). Therefore, from these observations it should be noted that the optimum amounts of ethyl bridge (15% ethyl) and bridge imidazolium moiety (10%) and concomitant control of plugs in the interior of the mesochannels of the catalyst are reached at a compromise between high catalyst activity and reaction selectivity (toward the formation of either aldehyde or carboxylic acid), most likely through a synergistic (cooperative) mechanism.

An alternative explanation may be also that for the plugged systems the effective diffusion of generated aldehyde from the system pores becomes lower in comparison with that for unplugged catalysts, giving rise to an enhanced concentration of aldehyde (or *gem*-diol) at available Pd active sites in the mesopores and thus causing its more pronounced reaction to the corresponding carboxylic acid.

In the final part of this study, the recyclability of either plugged or unplugged catalysts was examined in the aerobic oxidation of benzyl alcohol under the described reaction conditions. In this regard, after each reaction run, the catalysts Pd@U-E15 and Pd@P-E15 were recovered using simple filtration and reused for four subsequent reactions without any remarkable decrease in the catalyst activity and selectivity under the same reaction conditions (Figures S60 and S61 in the Supporting Information). To determine the leaching of Pd species into solution, a hot filtration test was performed. The Pd@P-E15 was filtered out after the aerobic oxidation of benzyl alcohol had run for 8 h (conversion 37%). The solid-free filtrate was then welded to another reaction vessel and continually stirred under standard reaction conditions (oxygen atmosphere, 90 °C). After 24 h, the analysis of the catalyst-free reaction showed that <3% benzoic acid was produced. This data was confirmed by atomic adsorption analysis of the filtrate solution and showed no Pd within the limit of detection (<1 ppm).

Scheme 3. Schematic Representation of Catalysts Pd@U-E15 (A) and Pd@P-E15 (B)

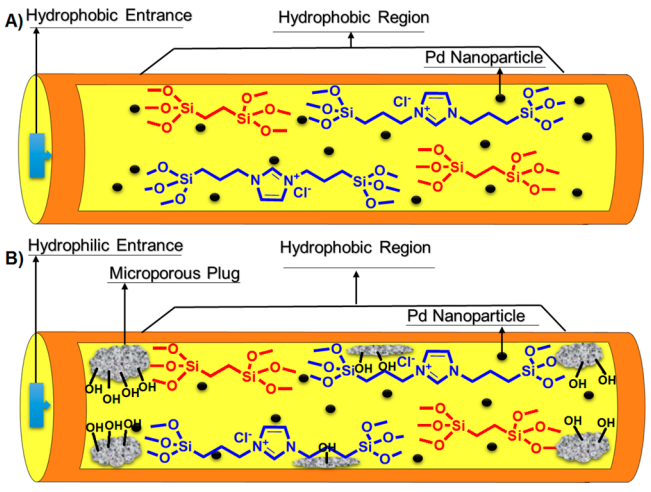

DOI: 10.1021/acscatal.5b00237
ACS Catal. 2015, 5, 4189–4200

To obtain information about the nature of the active Pd species in the aforementioned catalysts, samples of fresh and recovered catalyst Pd@P-E15 were studied using X-ray photoelectron spectroscopy (XPS). Figure 5 shows the XPS

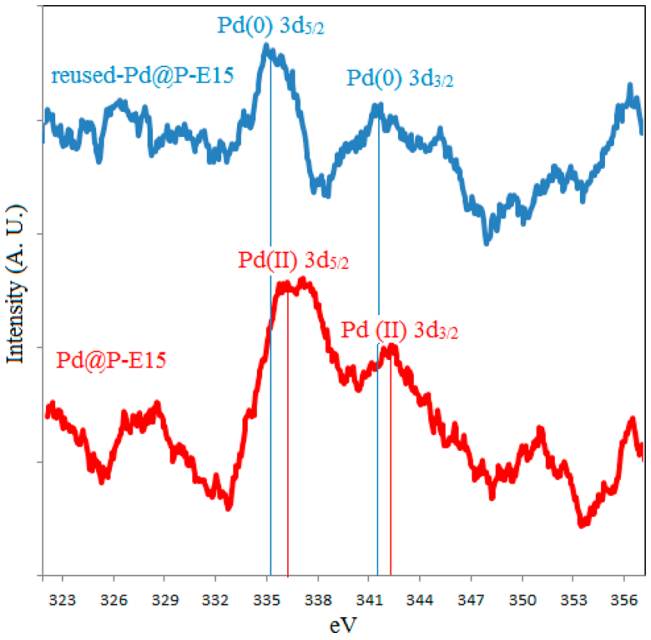

Figure 5. XPS spectra of the fresh and reused Pd@P-E15.

spectra of the region corresponding to the binding energy range of 320−360 eV, which includes Pd $3d_{3/2}$ and Pd $3d_{5/2}$ peaks. Predictably, the fresh catalyst Pd@P-E15 shows peaks located at 336 and 342 eV that were assigned to the Pd(II) $3d_{5/2}$ and Pd(II) $3d_{3/2}$ levels, respectively.[38] This binding energy clearly supported the Pd species in the fresh catalyst only as the Pd(II) form. On the other hand, the recovered catalyst Pd@P-E15 exhibited a similar pattern with slightly lower bonding energy which is evidence of the presence of the Pd catalyst in the metallic form.[38] Therefore, it is reasonable to speculate that the Pd species is most likely in the metallic form and the active component in our catalyst system.

Figure 6 is a typical TEM image of the recovered Pd@P-E-15 catalyst after the fourth reaction cycle. The image shows that

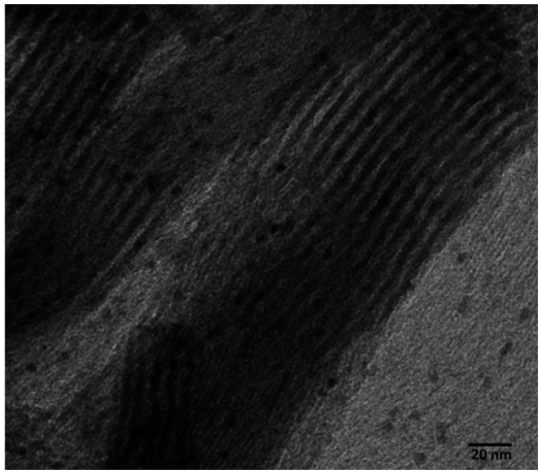

Figure 6. TEM image of recovered Pd@P-E15 (scale bar 20 nm).

the 2D-hexagonal structure of the pristine BFPMO-IL is mostly intact and Pd nanoparticles are well distributed throughout the regular channels. These findings clearly demonstrate that the mesoporous support provides the means for distributing and stabilizing the Pd nanoparticles inside the mesochannels of the catalyst system during the reaction.

CONCLUSION

We presented the preparation and characterization of a set of novel Pd catalysts based on plugged and unplugged bifunctional imidazolium-phenyl and -ethyl PMOs by varying the content of phenyl or ethyl bridges from 5 to 20%. Analysis showed that these materials have 2D *P6mm* symmetry with narrow pore size distributions and a varied degree of plugging in the mesopore channels. The coexistence of all described organic functionalities in the samples was successfully quantified by employing ^{13}C CP-MAS NMR, ^{29}Si CP-MAS NMR, DRIFT-IR, and elemental analysis, which also revealed that the relative organic contents can be varied within the indicated range without deterioration of the ordered structure. By modifying the condition of synthesis (stepwise addition of silica precursors) while keeping the PMO precursors contents similar to those of our plugged sample, we succeeded in preparing three unplugged bifunctional PMOs having 20% phenyl and 10% and 15% ethyl bridges, respectively. The catalytic activities of all catalysts were examined with the aim of identifying whether the surface physiochemical properties and the plugs could synergistically influence the selectivity of aerobic oxidation of primary benzylic alcohols. For the first time our studies show that varying the hydrophobic−hydrophilic balance with concomitant control of plugs in the interior of the mesochannels of the described catalyst enables tuning of both catalyst performance and reaction selectivity, possibly through a cooperative mechanism.

ASSOCIATED CONTENT

Supporting Information

The Supporting Information is available free of charge on the ACS Publications website at DOI: 10.1021/acscatal.5b00237.

Experimental details and additional data such as ^{1}H NMR, ^{13}C NMR, EDS, DRIFT-IR, TG, ^{29}Si CP-MAS NMR, ^{13}C CP-MAS NMR, SEM, TEM, N_2 and water adsorption−desorption isotherms, BJH pore size distributions, and gas chromatograms for the Tables 3 and 4 (PDF)

AUTHOR INFORMATION

Corresponding Author

*B.K.: fax, (+98-241-4214949); e-mail, Karimi@iasbs.ac.ir.

Notes

The authors declare no competing financial interest.

ACKNOWLEDGMENTS

The authors thank the Institute for Advanced Studies in Basic Science (IASBS), the Iran National Science Foundation (INSF) through Grant No. G014, and the Natural Science and Engineering Research Council (NSERC) of Canada for supporting this work. The assistance of Dr. David Liu and Dr. S. Kelly Sears at the Facility for Electron Microscopy Research is gratefully acknowledged.

DOI: 10.1021/acscatal.5b00237
ACS Catal. 2015, 5, 4189−4200

■ ABBREVIATIONS

PHTS, plugged hexagonal template silica; BTEB, 1,4-bis(triethoxysilyl)benzene; BTME, 1,2-bis(trimethoxysilyl)ethane; BTMSPCl, 1,3-bis(3-trimethoxysilylpropyl)imidazolium chloride; TMOS, tetramethoxyorthosilicate; TEOS, tetraethoxyorthosilicate; BFPMO, bifunctional periodic mesoporous organosilica; B*X*(5−20)-BFPMO-A, phenyl BFPMO composed of *X*% BTEB and synthesized according to method A (plugged phenyl BFPMOs); B*X*(5−20)-BFPMO-B, phenyl BFPMO composed of *X*% BTEB and synthesized according to method B (unplugged phenyl BFPMOs); E*X*(5−20)-BFPMO-A, ethyl BFPMO composed of *X*% BTME and synthesized according to method A (plugged ethyl BFPMOs); E*X*(10−20)-BFPMO-B, ethyl BFPMO composed of *X*% BTME and synthesized according to method B (unplugged ethyl BFPMOs); Pd@U-B20, palladium supported on B20-BFPMO-B (unplugged catalyst); Pd@U-E*X*, palladium supported on E*X*-BFPMO-B (unplugged catalyst); Pd@P-E*X*, palladium supported on E*X*-BFPMO-A (unplugged catalyst); Pd@PMO-Il, palladium supported on monofunctional PMO-IL

■ REFERENCES

(1) (a) Sheldon, R. A.; Kochi, J. K. *Metal-Catalyzed Oxidations of Organic Compounds*; Academic Press: New York, 1981. (b) Larock, R. C. *Comprehensive Organic Transformations*; Wiley-VCH: New York, 1989; pp 604−834. (c) Trost, B. M.; Fleming, I.; Ley, S. V. *Comprehensive Organic Synthesis*; Pergamon: Oxford, U.K., 1991; Vol. 7. (d) Dugger, R. W.; Ragan, J. A.; Ripin, D. H. B. *Org. Process Res. Dev.* **2005**, *9*, 253−258. (e) Carey, J. S.; Laffan, D.; Thomson, C.; Williams, M. T. *Org. Biomol. Chem.* **2006**, *4*, 2337−2347. (f) Ley, S. V.; Madfin, A. *Comprehensive Organic Synthesis*; Trost, B. M., Fleming, I., Ley, S. V., Eds.; Pergamon, Oxford, U. K., 1991; Vol. 7, pp 251−289.

(2) (a) Mallat, T.; Baiker, A. *Chem. Rev.* **2004**, *104*, 3037−3058. (b) Matsumoto, T.; Ueno, M.; Wang, N.; Kobayashi, S. *Chem. - Asian J.* **2008**, *3*, 196−214. (c) Karimi, B.; Zamani, A. *J. Iran. Chem. Soc.* **2008**, *5*, S1−S20. (d) Stratakis, M.; Garcia, H. *Chem. Rev.* **2012**, *112*, 4469−4506. (e) Dimitratos, N.; Lopez-Sanchez, J. A.; Hutchings, G. J. *Chem. Sci.* **2012**, *3*, 20−44.

(3) Mori, K.; Yamaguchi, K.; Hara, T.; Mizugaki, T.; Ebitani, K.; Kaneda, K. *J. Am. Chem. Soc.* **2002**, *124*, 11572−11573. (b) Jensen, D. R.; Schultz, M. J.; Mueller, J. A.; Sigman, M. S. *Angew. Chem., Int. Ed.* **2003**, *42*, 3810−3813. (c) Mori, K.; Hara, T.; Mizugaki, T.; Ebitani, K.; Kaneda, K. *J. Am. Chem. Soc.* **2004**, *126*, 10657−10666. (d) Pillai, U. R.; Sahle-Demessie, E. *Green Chem.* **2004**, *6*, 161−165. (e) Kwon, M. S.; Kim, N.; Park, C. M.; Lee, J. S.; Kang, K. Y.; Park, J. *Org. Lett.* **2005**, *7*, 1077−1079. (f) Karimi, B.; Zamani, Z.; Clark, J. H. *Organometallics* **2005**, *24*, 4695−4698. (g) Karimi, K.; Abedi, S.; Clark, J. H.; Budarin, V. *Angew. Chem., Int. Ed.* **2006**, *45*, 4776−4779. (h) Hara, K.; Tayama, S.; Kano, H.; Masuda, T.; Takakusagi, S.; Kondo, T.; Uosaki, K.; Sawamura, M. *Chem. Commun.* **2007**, 4280−4282. (i) Lu, A.-H.; Li, W.-C.; Hou, Z.; Schüth, F. *Chem. Commun.* **2007**, 1038−1040. (j) Hackett, S. F. J.; Brydson, R. M.; Gass, M. H.; Harvey, I.; Newman, A. D.; Wilson, K.; Lee, A. F. *Angew. Chem., Int. Ed.* **2007**, *46*, 8593−8596. (k) Chubarova, E. V.; Dickman, M. H.; Keita, B.; Nadjo, L.; Miserque, F.; Mifsud, M.; Arends, I. W. C. E.; Kortz, U. *Angew. Chem., Int. Ed.* **2008**, *47*, 9542−9546. (l) Hou, Z.; Theyssen, N.; Bronkmann, A.; Klementiev, K. V.; Grünert, W.; Bühl, M.; Schmidt, W.; Spliethoff, B.; Tesche, B.; Weidenthaler, C.; Leitner, W. *J. Catal.* **2008**, *258*, 315−323. (m) Samanta, S.; Nandi, A. K. *J. Phys. Chem. C* **2009**, *113*, 4721−4725. (n) Karimi, B.; Zamani, A.; Abedi, S.; Clark, J. H. *Green Chem.* **2009**, *11*, 109−119. (o) Hara, T.; Ishikawa, M.; Sawada, J.; Ichikuni, N.; Shimazu, S. *Green Chem.* **2009**, *11*, 2034−2040. (p) Polshettiwar, V.; Varma, R. S. *Org. Biomol. Chem.* **2009**, *7*, 37−40. (q) Barats, D.; Neumann, R. *Adv. Synth. Catal.* **2010**, *352*, 293−298. (r) Banda; Aggarwal, N.; Das, P. *Tetrahedron Lett.* **2011**, *52*, 4954−4956. (s) Parlett, C. M. A.; Bruce, D. W.; Hondow, N. S.; Newton, M. A.; Lee, A. F.; Wilson, K. *ChemCatChem* **2013**, *5*, 939−950. (t) Johnston, E. V.; Verho, O.; Kärkäs, M. D.; Shakeri, M.; Tai, C.-W.; Palmgren, P.; Eriksson, K.; Oscarsson, S.; Bäckvall, J. E. *Chem. - Eur. J.* **2012**, *18*, 12202−12206. (w) Karimi, B.; Behzadnia, H.; Bostina, M.; Vali, H. *Chem. - Eur. J.* **2012**, *18*, 8634−8640. (x) Ravat, V.; Nongwe, I.; Meijboom, R.; Bepete, G.; Coville, N. J. *J. Catal.* **2013**, *305*, 36−45.

(4) (a) Yamada, Y. M. A.; Arakawa, T.; Hocke, H.; Uozumi, Y. *Angew. Chem., Int. Ed.* **2007**, *46*, 704−706. (b) Wang, T.; Xiao, C. X.; Yan, L.; Xu, L.; Luo, J.; Shou, H.; Kou, Y.; Liu, H. *Chem. Commun.* **2007**, 4375−4377. (c) Miyamura, C.; Matsubara, R.; Kobayashi, S. *Chem. Commun.* **2008**, 2031−2033. (d) Ng, Y. H.; Ikeda, S.; Morita, Y.; Harada, T.; Ikeue, K.; Matsumura, M. *J. Phys. Chem. C* **2009**, *113*, 12799−12805.

(5) (a) Abad, A.; Concepción, C.; Corma, A.; Garcia, H. *Angew. Chem., Int. Ed.* **2005**, *44*, 4066−4069. (b) Su, F. Z.; Liu, Y. M.; Wang, L. C.; Cao, Y.; He, H. Y.; Fan, K. N. *Angew. Chem., Int. Ed.* **2008**, *47*, 334−337. (c) Mitsudome, T.; Noujima, A.; Mizugaki, T.; Jitsukawa, K.; Kaneda, K. *Adv. Synth. Catal.* **2009**, *351*, 1890−1896. (d) Lucchesi, C.; Inasaki, T.; Miyamura, H.; Matsubara, R.; Kobayashi, S. *Adv. Synth. Catal.* **2008**, *350*, 1996−2000. (e) Wang, X.; Kawanami, H.; Islam, N. M.; Chattergee, M.; Yokoyama, T.; Ikushima, T. *Chem. Commun.* **2008**, 4442−4444. (f) Miyamura, H.; Matsubara, R.; Miyazaki, Y.; Kobayashi, S. *Angew. Chem., Int. Ed.* **2007**, *46*, 4151−4154. (g) Karimi, B.; Kabiri Esfahani, F. *Chem. Commun.* **2009**, 5555−5557. (h) Tsunoyama, H.; Sakurai, H.; Negishi, Y.; Tsukuda, T. *J. Am. Chem. Soc.* **2005**, *127*, 9374−9375. (i) Kanaoka, S.; Yagi, N.; Fukuyama, Y.; Aoshima, S.; Tsunoyama, H.; Tsukuda, T.; Sakurai, H. *J. Am. Chem. Soc.* **2007**, *129*, 12060−12061. (j) Kim, S.; Bae, S. W.; Lee, J. S.; Park, J. *Tetrahedron* **2009**, *65*, 1461−1466. (k) Kaizuka, K.; Miyamura, H.; Kobayashi, S. *J. Am. Chem. Soc.* **2010**, *132*, 15096−15098.

(6) (a) Yamaguchi, K.; Mori, K.; Mizugaki, T.; Ebitani, K.; Kaneda, K. *J. Am. Chem. Soc.* **2000**, *122*, 7144−7145. (b) Yamaguchi, K.; Mizuno, N. *Angew. Chem., Int. Ed.* **2002**, *41*, 4538−4542. (c) Ebitani, K.; Motokura, K.; Mizugaki, T.; Kaneda, K. *Angew. Chem., Int. Ed.* **2005**, *44*, 3423−3426. (d) Kotani, M.; Koike, T.; Yamaguchi, K.; Mizuno, N. *Green Chem.* **2006**, *8*, 735−741. (e) Mori, K.; Kanai, S.; Hara, T.; Mizugaki, T.; Ebitani, K.; Jitsukawa, K.; Kaneda, K. *Chem. Mater.* **2007**, *19*, 1249−1256. (f) Mondelli, C.; Ferri, D.; Baiker, A. *J. Catal.* **2008**, *258*, 170−176. (g) Mori, S.; Takubo, M.; Makida, K.; Yanase, T.; Aoyagi, S.; Maegawa, T.; Monguchi, Y.; Sajiki, H. *Chem. Commun.* **2009**, 5159−5161.

(7) (a) Markó, I. E.; Giles, P. R.; Tsukazaki, M.; Brown, S. M.; Urch, C. J. *Science* **1996**, *274*, 2044−2046. (b) Gamez, P.; Arends, I.W. C. E.; Reedijka, J.; Sheldon, R. A. *Chem. Commun.* **2003**, 2414−2415. (c) Jiang, N.; Ragauskas, A. J. *ChemSusChem* **2008**, *1*, 823−825. (d) Lina, L.; Juanjuana, M.; Liuyana, J.; Yunyang, W. *J. Mol. Catal. A: Chem.* **2008**, *291*, 1−4.

(8) (a) Fey, T.; Fischer, H.; Bachman, S.; Albert, K.; Bolm, C. *J. Org. Chem.* **2001**, *66*, 8154−8159. (b) Pozzi, G.; Cavazzini, M.; Quici, S.; Benagli, M.; Anna, G. D. *Org. Lett.* **2004**, *6*, 441−443. (c) Liu, R. H.; Liang, X. M.; Dong, C. Y.; Hu, X. Q. *J. Am. Chem. Soc.* **2004**, *126*, 4112−4113. (d) Liu, R. H.; Dong, C. Y.; Liang, X. M.; Wang, X. J.; Hu, X. Q. *J. Org. Chem.* **2005**, *70*, 729−731. (e) Gheorghe, A.; Matsuno, A.; Reiser, O. *Adv. Synth. Catal.* **2006**, *348*, 1016−1020. (f) Karimi, B.; Biglari, A.; Clark, J. H.; Budarin, V. *Angew. Chem., Int. Ed.* **2007**, *46*, 7210−7213. (g) Xie, Y.; Mo, W. M.; Xu, D.; Shen, Z. L.; Sun, N.; Hu, B. X.; Hu, X. Q. *J. Org. Chem.* **2007**, *72*, 4288−4291. (h) Wang, X. L.; Liu, R. H.; Jin, Y.; Liang, X. M. *Chem. - Eur. J.* **2008**, *14*, 2679−2685. (i) He, X. J.; Shen, Z. L.; Mo, W. M.; Sun, N.; Hu, B. X.; Hu, X. Q. *Adv. Synth. Catal.* **2009**, *351*, 89−92. (j) Karimi, B.; Badreh, E. *Org. Biomol. Chem.* **2011**, *9*, 4194−4198. (k) Karimi, B.; Farhangi, E. *Chem. - Eur. J.* **2011**, *17*, 6056−6060. (l) Karimi, B.; Farhangi, E.; Vali, H.; Vahdati, S. *ChemSusChem* **2014**, *7*, 2735−2741.

(9) Wang, T.; Shou, H.; Kou, Y.; Liu, H. *Green Chem.* **2009**, *11*, 562−568.

(10) Korovchenko, P.; Donze, C.; Gallezot, P.; Besson, M. *Catal. Today* **2007**, *121*, 13−21.

DOI: 10.1021/acscatal.5b00237
ACS Catal. 2015, 5, 4189−4200

(11) (a) Asefa, T.; MacLachlan, M. J.; Coombs, N.; Ozin, G. A. *Nature* **1999**, *402*, 867−871. (b) Yoshina-Ishii, C.; Asefa, T.; Coombs, N.; MacLachlan, M. J.; Ozin, G. A. *Chem. Commun.* **1999**, 2539−2540. (c) Melde, B. J.; Holland, B. T.; Blanford, C. F.; Stein, A. *Chem. Mater.* **1999**, *11*, 3302−3308. (d) Inagaki, S.; Guan, S.; Fukushima, Y.; Ohsuna, T.; Terasaki, O. *J. Am. Chem. Soc.* **1999**, *121*, 9611−9614.

(12) For catalysis based on PMOs see: (a) Clark, J. H.; Macquarrie, d. J.; Tavener, S. J. *Dalton Trans.* **2006**, 4297−4309. (b) Shylesh, S.; Samuel, P.; Sisodiya, S.; Singh, A. P. *Catal. Surv. Asia* **2008**, *12*, 266−282. (c) Yang, Q.; Liu, J.; Zhang, L.; Li, C. *J. Mater. Chem.* **2009**, *19*, 1945−1955. (d) De Canck, E.; Varcaemst, C.; Verpoort, F.; Van Der Voort, P. *Stud. Surf. Sci. Catal.* **2010**, *175*, 365−368. (e) Jeong, E.-Y.; Burri, A.; Lee, S.-Y.; Park, S.-E. *J. Mater. Chem.* **2010**, *20*, 10869−10875. (f) Thomas, A. *Angew. Chem., Int. Ed.* **2010**, *49*, 8328−8344. (g) Mizoshita, N.; Tani, T.; Inagaki, S. *Chem. Soc. Rev.* **2011**, *40*, 789−800. (h) Wang, L.; Shylesh, S.; Dehe, D.; Philippi, T.; Dörr, G.; Seifert, A.; Zhou, Z.; Hartmann, M.; Klupp Taylor, R. N.; Jia, M.; Ernst, S.; Thiel, W. R. *ChemCatChem* **2012**, *4*, 395−400. (i) Karimi, B.; Kabiri Esfahani, F. *Adv. Synth. Catal.* **2012**, *354*, 1319−1326. (j) Van Der Voort, P.; Esquivel, D.; De Canck, E.; Goethals, F.; Van Driessche, I.; Romero-Salguero, F. J. *Chem. Soc. Rev.* **2013**, *42*, 3913−3955. (k) Díaz, U.; Brunel, D.; Corma, A. *Chem. Soc. Rev.* **2013**, *42*, 4083−4097. (l) De Canck, E.; Dosuna-Rodriguez, I.; Gaigneaux, E. M.; Van Der Voort, P. *Materials* **2013**, *6*, 3556−3570. (m) Elhamifar, D.; Shábani, A. *Chem. - Eur. J.* **2014**, *20*, 3212−3217. (n) Prasad, A. N.; Reddy, B. M.; Jeong, E.-Y.; Park, S.-E. *RSC Adv.* **2014**, *4*, 29772−29781. (o) Wang, J.; Zou, Y.; Sun, Y.; Hemgesberg, M.; Schaffner, D.; Gao, H.; Zhang, W.; Jia, M.; Thiel, W. R. *Chin. J. Catal.* **2014**, *35*, 532−539. For other applications see: (p) Lu, Y. F.; Fan, H. Y.; Doke, N.; Loy, D. A.; Assink, R. A.; LaVan, D. A.; Brinker, C. J. *J. Am. Chem. Soc.* **2000**, *122*, 5258−5261. (q) Burleigh, M. C.; Dai, S.; Hagaman, E. W.; Lin, J. S. *Chem. Mater.* **2001**, *13*, 2537−2546. (r) Zhu, G. R.; Yang, Q. H.; Jiang, D. M.; Yang, J.; Zhang, L.; Li, Y.; Li, C. *J. Chromatogr. A* **2006**, *1103*, 257−264. (s) Olkhovyk, O.; M. Jaroniec, M. *Ind. Eng. Chem. Res.* **2007**, *46*, 1745−1751. (t) Comotti, A.; Bracco, S.; Valsesia, P.; Ferretti, L.; Sozzani, P. *J. Am. Chem. Soc.* **2007**, *129*, 8566−8576. (u) Zhu, G. R.; Jiang, D. M.; Yang, Q. H.; Yang, J.; Li, C. *J. Chromatogr. A* **2007**, *1149*, 219−227. (w) Wang, X. Q.; Lu, D. N.; Austin, R.; Agarwal, A.; Mueller, L. J.; Liu, Z.; Wu, J. Z.; Feng, P. Y. *Langmuir* **2007**, *23*, 5735−5739. (x) E, -B. Cho.; Kim, D.; Jaroniec, M. *Langmuir* **2009**, *25*, 13258−13263. (y) Wang, W. D.; Grozea, D.; Kohli, S.; Perovic, D. D.; Ozin, G. A. *ACS Nano* **2011**, *5*, 1267−1275. (z) Vathyam, R.; Wondimu, E.; Das, S.; Zhang, C.; Hayes, S.; Tao, Z. M.; Asefa, T. *J. Phys. Chem. C* **2011**, *115*, 13135−13150. (aa) Ravanan, M.; Ghaedi, M.; Ansari, A.; Taghizadeh, F.; Elhamifar, D. *Spectrochim. Acta, Part A* **2014**, *123*, 467−471. (bb) Ghaedi, M.; Elhamifar, D.; Roosta, M.; Moshgelgosha, R. *J. Ind. Eng. Chem.* **2014**, *20*, 1703−1712.

(13) (a) Park, M.; Park, S. S.; Selvaraj, M.; Zhao, D. Y.; Ha, C. S. *Microporous Mesoporous Mater.* **2009**, *124*, 76−83. (b) Arcos, D.; López-Noriega, A.; Ruiz-Hernández, E.; Terasaki, O.; Vallet-Regí, M. *Chem. Mater.* **2009**, *21*, 1000−1009. (c) Parambadath, S.; Rana, V. K.; Zhao, D. Y.; Ha, C. S. *Microporous Mesoporous Mater.* **2011**, *141*, 94−101. (d) Russo, P. A.; Carrott, M. M. L. R.; Carrott, P. J. M. *New J. Chem.* **2011**, *35*, 407−416. (e) Zhu, L.; Liu, X.; Chen, T.; Xu, Z.; Yan, W.; Zhang, H. *Appl. Surf. Sci.* **2012**, *258*, 7126−7134.

(14) (a) Van Der Voort, P.; Ravikovitch, P. I.; De Jong, K. P.; Neimark, A. V.; Janssen, A. H.; Benjelloun, M.; Van Bavel, E.; Cool, P.; Weckhuysen, B. M.; Vansant, E. F. *Chem. Commun.* **2002**, 1010−1011. (b) Van Der Voort, P.; Ravikovitch, P. I.; De Jong, K. P.; Benjelloun, M.; Van Bavel, E.; Janssen, A. H.; Neimark, A. V.; Weckhuysen, B. M.; Vansant, E. F. *J. Phys. Chem. B* **2002**, *106*, 5873−5877. (c) Vercaemst, C.; Ide, M.; Friedrich, H.; de Jong, K. P.; Verpoort, F.; Van Der Voort, P. *J. Mater. Chem.* **2009**, *19*, 8839−8845. (d) Vercaemst, C.; Ide, M.; Friedrich, H.; de Jongh, P. E.; Neimark, A. V.; Goderis, B.; Verpoort, F.; Van Der Voort, P. *J. Phys. Chem. C* **2009**, *113*, 5556−5562.

(15) (a) Min, B.-H.; Jeong, E.-Y.; Thommes, M.; Park, S.-E. *Chem. Commun.* **2011**, *47*, 4673−4675. (b) Wang, W.; Shan, W.; Ru, H.; Wang, N. W. *J. Mater. Chem.* **2011**, *21*, 12059−12067. (c) Shan, W.; Ru, H. *J. Mater. Chem.* **2011**, *21*, 17433−17440. For mechanism of plug formation also see: (d) Kruk, M.; Jaroniec, M.; Joo, S. H.; Ryoo, R. *J. Phys. Chem. B* **2003**, *107*, 2205−2213.

(16) Celer, E. B.; Kruk, M.; Zuzek, Y.; Jaroniec, M. *J. Mater. Chem.* **2006**, *16*, 2824.

(17) (a) Lee, J.; Park, Y.; Kim, P.; Kim, H.; Yi, J. *J. Mater. Chem.* **2004**, *14*, 1050−1056. (b) Celer, E. B.; Kruk, M.; Zuzek, Y.; Jaroniec, M. *J. Mater. Chem.* **2006**, *16*, 2824−2833. (c) Reddy, S. S.; Kumar, V. S.; Padmasri, A. H.; Satyanarayana, C. V. V; Raju, B. D.; Rao, K. S. R. *Catal. Commun.* **2007**, *8*, 1080−1087. (d) Wu, Z. Y.; Wang, H. J.; Zhuang, T. T.; Sun, L. B.; Wang, Y. M.; Zhu, J. H. *Adv. Funct. Mater.* **2008**, *18*, 82−94. (e) Zukal, A.; Siklová, H.; Cejka, J. *Langmuir* **2008**, *24*, 9837−9842. (f) Wu, Z. Y.; Wang, H. J.; Zhuang, T. T.; Sun, L. B.; Wang, Y. M.; Zhu, J. H. *Adv. Funct. Mater.* **2008**, *18*, 82−94. (g) Prasetyanto, E. A.; Lee, S.-C.; Jeong, S.-M.; Park, S.-E. *Chem. Commun.* **2008**, 1995−1997. (h) Rasmussen, C. J.; Vishnyakov, A.; Thommes, M.; Smarsly, B. M.; Kleitz, F.; Neimark, A. V. *Langmuir* **2010**, *26*, 10147−10157. (i) Min, B.-H.; Jeong, E.-Y.; Thommes, M.; Park, S.-E. *Chem. Commun.* **2011**, *47*, 4673−4675. (j) Prasetyanto, E. A.; Jeong, S.-M.; Park, S.-E. *Top. Catal.* **2010**, *53*, 192−199. (k) Jeong, E.-Y.; Lim, C.-R.; Jin, H.; Park, S.-E. *Chem. Commun.* **2012**, *48*, 3079−3081. (l) Shakeri, M.; Gebbink, R. J. M. K.; de Jongh, P. E.; de Jong, K. P. *Angew. Chem., Int. Ed.* **2013**, *52*, 10854−10857.

(18) (a) Karimi, B.; Zareyee, D. *Org. Lett.* **2008**, *10*, 3989−3992. (b) Karimi, B.; Zareyee, D. *J. Mater. Chem.* **2009**, *19*, 8665−8670. (c) Karimi, B.; M. Mirzaei, H.; Mobaraki, A. *Catal. Sci. Technol.* **2012**, *2*, 828−834. (d) Karimi, B.; M. Mirzaei, H. *RSC Adv.* **2013**, *3*, 20655−20661. (e) Karimi, B.; Mobaraki, A.; M. Mirzaei, H.; Zareyee, D.; Vali, H. *ChemCatChem* **2014**, *6*, 212−219. (f) Karimi, B.; Khorasani, M. *ACS Catal.* **2013**, *3*, 1657−1664. For water-tolerant magnetic nanocatalysts also see: (g) Mobaraki, A.; Movassagh, B.; Karimi, B. *ACS Comb. Sci.* **2014**, *16*, 352−358. (h) Mobaraki, A.; Movassagh, B.; Karimi, B. *Appl. Catal., A* **2014**, *472*, 123−133.

(19) (a) Karimi, B.; Elhamifar, D.; Clark, J. H.; Hunt, A. J. *Chem. - Eur. J.* **2010**, *16*, 8047−8053. (b) Karimi, B.; Gholinejad, M.; Khorasani, M. *Chem. Commun.* **2012**, *48*, 8961−8963. (c) Elhamifar, D.; Karimi, B.; Rastegar, J.; Banakar, M. H. *ChemCatChem* **2013**, *5*, 2418−2424. (d) Karimi, B.; Bakhshandeh Rostami, F.; Khorasani, M.; Elhamifar, D.; Vali, H. *Tetrahedron* **2014**, *70*, 6114−6119. (e) Nasr-Esfahani, M.; Elhamifar, D.; Amadeh, T.; Karimi, B. *RSC Adv.* **2015**, *5*, 13087−13094. (f) Elhamifar, D.; Hosseinpoor, F.; Karimi, B.; Hajati, S. *Microporous Mesoporous Mater.* **2015**, *204*, 269−275. (g) Karimi, B.; Khorasani, M.; Bakhshandeh Rostami, F.; Elhamifar, D.; Vali, H. *ChemPlusChem* **2015**, *80*, 990−999. For organocatalysts based on PMO-IL also see: (h) Elhamifar, D.; Nasr-Esfahani, M.; Karimi, B.; Moshgelgosha, R.; Shábani, A. *ChemCatChem* **2014**, *6*, 2593−2599. (i) Elhamifar, D.; Karimi, B.; Moradi, A.; Rastegar, J. *ChemPlusChem* **2014**, *79*, 1147−1152.

(20) (a) Hou, Z. S.; Theyssen, N.; Leitner, W. *Green Chem.* **2007**, *9*, 127−132. (b) Hu, J.; Chen, L.; Zhu, K.; Suchopar, A.; Richards, R. *Catal. Today* **2007**, *122*, 277−283. (c) Matdumoto, T.; Ueno, M.; Wang, N.; Kobayashi, S. *Chem. - Asian J.* **2008**, *3*, 196−214. (d) Liu, Y.; Tsunoyama, H.; Akita, T.; Tsukuda, T. *J. Phys. Chem. C* **2009**, *113*, 13457−13461. (e) Ma, C. Y.; Dou, B. J.; Cheng, J.; Hu, Q.; Hao, Z. P.; Qiao, Z. S. *Appl. Catal., B* **2009**, *92*, 202−208. (f) Liu, Y. M.; Tsunoyama, H.; Akita, T.; Tsukuda, T. *Chem. Lett.* **2010**, *39*, 159−161. (g) Yang, H.; Han, X.; Ma, Z.; Wang, R.; Liu, J.; Ji, X. *Green Chem.* **2010**, *12*, 441−451. (h) Stratakis, M.; Garcia, H. *Chem. Rev.* **2012**, *112*, 4469−4506. (i) Dimitratos, N.; Lopez-Sanchez, J. A.; Hutchings, G. J. *Chem. Sci.* **2012**, *3*, 20−44. (j) Parmeggiani, C.; Cardona, F. *Green Chem.* **2012**, *4*, 547−564. (k) Dalla Pina, C.; Falletta, E.; Rossi, M. *Chem. Soc. Rev.* **2012**, *41*, 350−369. (l) Liu, J.; Yang, H. Q.; Klietz, F.; Chen, Z. G.; Yang, T.; Strounia, E.; Lu, G. Q.; Qiao, S. Z. *Adv. Funct. Mater.* **2012**, *22*, 591−599. (m) Opanasenko, M.; Štěpnička, P.; Čejka, J. *RSC Adv.* **2014**, *4*, 65137−65162.

(21) See the Supporting Information for details. Among the pristine BFPMO materials that were used in this study, B5-BFPMO-A, E10-BFPMO-A, E15-BFPMO-B, and B20-BFPMO-B were previously reported in our recent publication:. Karimi, B.; Khorasani, M.; Vali, H.; Luque, R. *J. Mater. Chem. A* **2015**, *3*, 6575−6585.

DOI: 10.1021/acscatal.5b00237
ACS Catal. 2015, 5, 4189−4200

(22) Karimi, B.; Elhamifar, D.; Yari, O.; Khorasani, M.; Vali, H.; Clark, J. H.; Hunt, A. J. *Chem. - Eur. J.* **2012**, *18*, 13520−13530.
(23) (a) Everett, D. H.; Gregg, S. J.; Sing, K. S. W.; Stoeckli, H. F. *Characterization of Porous Solids*; Soc. Chem. Ind.: London, 1979; p 229. (b) Seaton, N. A. *Chem. Eng. Sci.* **1991**, *46*, 1895−1909. (c) Groen, J. C.; Peffer, L. A. A.; Pérez-Ramírez, J. *Microporous Mesoporous Mater.* **2003**, *60*, 1−17. (d) Landers, J.; Gor, G. Y.; Neimark, A. V. *Colloids Surf., A* **2013**, *437*, 3−32.
(24) (a) Wang, W.; Zhou, W.; Sayari, A. *Chem. Mater.* **2003**, *15*, 4886−4889. (b) Cho, E. B.; Han, O. H.; Kim, S.; Kim, D.; Jaroniec, M. *Chem. Commun.* **2010**, *46*, 4568−4570.
(25) Hamoudi, S.; Yang, Y.; Moudrakovski, I. L.; Lang, S.; Sayari, A. *J. Phys. Chem. B* **2001**, *105*, 9118−9123.
(26) (a) Bao, X. Y.; Zhao, X. S.; Li, X.; Chia, P. A.; Li, J. *J. Phys. Chem. B* **2004**, *108*, 4684−4689. (b) Liang, Y.; Hanzlik, M.; Anwander, R. *Chem. Commun.* **2005**, 525−527. (d) Zhang, W.-H.; Daly, B.; OCallaghan, J.; Zhang, L.; Shi, J.-L.; Li, C.; Morris, M. A.; Holmes, J. D. *Chem. Mater.* **2005**, *17*, 6407−6415.
(27) (a) Zhang, L.; Liu, J.; Yang, J.; Yang, Q.; Li, C. *Microporous Mesoporous Mater.* **2008**, *109*, 172−183. (b) Zhu, F.-X.; Wang, W.; Li, H.-X. *J. Am. Chem. Soc.* **2011**, *133*, 11632−11640.
(28) Alauzun, J.; Mehdi, A.; Reyé, C.; Corriu, R. J. P. *J. Mater. Chem.* **2007**, *17*, 349−356.
(29) Temtsin, G.; Asefa, T.; Bittner, S.; Ozin, G. A. *J. Mater. Chem.* **2001**, *11*, 3202−3206.
(30) Burleigh, M. C.; Markowitz, M. A.; Spector, M. S.; Gaber, B. P. *J. Phys. Chem. B* **2001**, *105*, 9935−9942.
(31) (a) Karimi, B.; Enders, D. *Org. Lett.* **2006**, *8*, 1237−1240. (b) Bordoloi, A.; Sahoo, S.; Lefebvre, F.; Halligudi, S. B. *J. Catal.* **2008**, *259*, 232−239. (c) Jin, Y.; Wang, P. J.; Yin, D. H.; Liu, J. F.; Qiu, H. Y.; Yu, N. Y. *Microporous Mesoporous Mater.* **2008**, *111*, 569−576.
(32) Esquivel, D.; Jimenez-Sanchidrian, C.; Romero-Salguero, F. J. *Mater. Lett.* **2011**, *65*, 1460−1464.
(33) (a) Karimi, B.; Ghoreishi-Nezhad, M.; Clark, J. H. *Org. Lett.* **2005**, *7*, 625−628. (b) Karimi, B.; Mansouri, F.; Vali, H. *Green Chem.* **2014**, *16*, 2587−2596.
(34) Karimi, B.; Elhamifar, D.; Clark, J. H.; Hunt, A. *Org. Biomol. Chem.* **2011**, *9*, 7420−7426.
(35) Burleigh, M. C.; Markowitz, M. A.; Jayasundera, S.; Spector, M. S.; Thomas, C. W.; Gaber, B. P. *J. Phys. Chem. B* **2003**, *107*, 12628−12634.
(36) Tang, L.; Guo, X.; Li, Y.; Zhang, S.; Zha, Z.; Wang, Z. *Chem. Commun.* **2013**, *49*, 5213−5215.
(37) Sankar, M.; Nowicka, E.; Carter, E.; Murphy, D. M.; Knight, D. W.; Bethell, D.; Hutchings, G. J. *Nat. Commun.* **2014**, *5*, 3765−3768.
(38) Yang, H.; han, X.; Li, G.; Ma, Z.; Hao, Y. *J. Phys. Chem. C* **2010**, *114*, 22221−22229.

DOI: 10.1021/acscatal.5b00237
ACS Catal. 2015, 5, 4189−4200